

See discussions, stats, and author profiles for this publication at: <https://www.researchgate.net/publication/316210079>

Calcification on mortar by live and UV-killed biofilm-forming cyanobacterial *Gloeocapsa* PCC73106

Article in *Construction and Building Materials* · August 2017

DOI: 10.1016/j.conbuildmat.2017.04.026

CITATION

1

READS

294

3 authors:



Tingting Zhu

University of Toronto

12 PUBLICATIONS **91** CITATIONS

[SEE PROFILE](#)



Xiancai Lu

Nanjing University

141 PUBLICATIONS **1,236** CITATIONS

[SEE PROFILE](#)



Maria Dittrich

University of Toronto

74 PUBLICATIONS **1,353** CITATIONS

[SEE PROFILE](#)

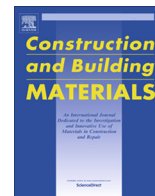
Some of the authors of this publication are also working on these related projects:



Clay Minerals [View project](#)



Goldschmidt 2017 session 15i: MICROBIAL BIOMINERALIZATION: MECHANISMS, IMPACTS AND APPLICATIONS [View project](#)



Calcification on mortar by live and UV-killed biofilm-forming cyanobacterial *Gloeocapsa* PCC73106



Tingting Zhu^a, Xiancai Lu^b, Maria Dittrich^{a,*}

^a Department of Physical and Environmental Sciences, University of Toronto Scarborough, 1265 Military Trail, Toronto, Ontario M1C 1A4, Canada

^b School of Earth Sciences and Engineering, Nanjing University, 163 Xianlin Road, Qixia District, Nanjing, Jiangsu 210023, China

HIGHLIGHTS

- Cyanobacteria *Gloeocapsa* PCC73106 under illumination led to most calcification.
- UV-killed cells improved the mortar durability the most.
- Extracellular polymeric substances helped the cells adhere to the mortar cubes.

ARTICLE INFO

Article history:

Received 22 November 2016

Received in revised form 11 March 2017

Accepted 5 April 2017

Keywords:

Mortar

Microbial carbonate precipitation

Cyanobacteria *Gloeocapsa* PCC73106

UV-killed cell

Biofilm

ABSTRACT

Microbial carbonate precipitation by phototrophic cyanobacteria in mortars enhances their durability. This study investigated the calcification by cyanobacteria *Gloeocapsa* PCC73106 in mortars. The calcium concentration and the pH were monitored, the carbonate precipitates were observed, and the performances of cubes were evaluated. Treatments with live cells under illumination resulted in the largest amount of precipitates, while UV-killed cells contributed to the highest compressive strength, the least water absorption and the lowest porosity. The morphology of precipitates differs greatly under different conditions. This is the first study showing that UV-killed *Gloeocapsa* PCC73106 can be a potential candidate for improving the performance of mortars.

© 2017 Elsevier Ltd. All rights reserved.

1. Introduction

Microbial carbonate precipitation (MCP) plays important roles in metal coprecipitation and cementation in natural systems [1,2]. A number of biotechnologies based on MCP have been applied in metal remediation, carbon sequestration and construction restoration [3–5]. The use of MCP in mortars has been proposed, despite the challenge of the extremely high pH in environmental fluids [6]. The improvement of the compressive strength, enhancement of the durability and a decrease of water absorption have been observed in laboratory studies [7].

Ureolytic bacteria have been primarily investigated in the emerging microbial concrete technology [8,9]. An alternative technology involving autophototrophic cyanobacteria, instead of ureolytic bacteria, was recently introduced by our research group, and only one study has been published so far [10]. The technology

using ureolytic bacteria is highly dependent on the metabolic activity of ureolysis, which means that cells have to be alive to promote the precipitation of carbonates. Additionally, the metabolic activity of ureolytic bacteria leads to a production of nitrogen compounds, such as air pollutant NH₃. The use of a variety of live bacteria, however, is restricted in diverse circumstances; therefore, killed cells have to be considered [11].

In contrast, cyanobacteria have a greater mucilage production that improves the affinity between cells and inorganic matrix. Furthermore, the culturing of autotrophic cyanobacteria only requires easily prepared nutrient solutions, and cyanobacteria are cosmopolitan, living in a wide range of environments, from the Arctic to deserts. While photosynthesis by cyanobacteria was reported to promote the calcification, it does not influence the early stage of the calcification process, the nucleation process [12]. Consequently, both live and dead cyanobacteria cells have led to carbonate precipitation [13]. All these specific features make the cyanobacterial carbonate production (CCP) technology less expensive, more advanced and sustainable [11]. Thus, there is an urgent

* Corresponding author.

E-mail addresses: tingting.zhu@mail.utoronto.ca (T. Zhu), xcljun@nju.edu.cn (X. Lu), mdittrich@utsc.utoronto.ca (M. Dittrich).

need for in-depth investigations of autotrophic cyanobacteria for technological applications.

Gloeocapsa, a biofilm-forming cyanobacteria, is the most widespread cyanobacteria occurring on natural carbonate substratum such as marble and limestone monuments [14]. The optimal pH for their growth is 7–8 [15]. The gelatinous sheath of *Gloeocapsa* not only acts as a reservoir of water and protects them from dry conditions but also helps them to adhere to the substratum [14]. Live and dead *Gloeocapsa* cells showed high laboratory calcification rates in monoculture without heterotrophic bacterial component [16], however, the potential of *Gloeocapsa* for MCP in mortars has not been studied so far.

In this study, the performance of mortars treated abiotically, with live *Gloeocapsa* PCC73106 (*Gloe.* PCC73106) cells under illumination, with live cells under darkness and with UV-killed cells, was investigated. The comparison of the experimental results under these conditions revealed the relative importance of extracellular polymeric substances (EPS), cell surfaces, photosynthesis and other metabolic activities on the carbonate precipitation. The surface and mechanical properties of mortars with different treatments showed that the performance of mortar cubes treated with UV-killed cells outperforms the others.

2. Material and methods

2.1. Culture conditions

A biofilm-forming cyanobacteria, *Gloe.* PCC73106, was received from Pasteur Culture Collection and grown in BG-11 medium (comprised of NaNO₃ 17.6 mM, K₂HPO₄ 0.23 mM, MgSO₄·7H₂O 0.3 mM, CaCl₂·2H₂O 0.24 mM, citric acid·H₂O 0.031 mM, ferric ammonium citrate 0.021 mM, Na₂EDTA·2H₂O 0.0027 mM, Na₂CO₃ 0.19 mM and BG-11 trace metal H₃BO₃ 46 mM, MnCl₂·4H₂O 9 mM, ZnSO₄·7H₂O 0.77 mM, Na₂MoO₄·2H₂O 1.6 mM, CuSO₄·5H₂O 0.3 mM, Co(NO₃)₂·6H₂O 0.17 mM). Batch cultures were constantly shaken at 110 rpm under the room temperature of 22 ± 1 °C with a light intensity of 20 μE m⁻² s⁻¹ (HOBO Micro Station H21-002 light sensor).

After reaching the stationary growth stage, cells were collected by centrifuging at 7200 rpm for 15 min. Just before the experiments, cell washes were carried out in a sterilized 0.1 M NaNO₃ solution through 3 cycles of centrifuging, discarding the supernatant and resuspending in the 0.1 M NaNO₃ solution. After the last wash, cells were resuspended in deionized water. One-third of the cell suspension was exposed to UV light for 1 h to be killed, while the rest was kept for the experiments. While being exposed to UV light, some cyanobacteria such as *Gloeocapsa* sp. produce more EPS as a stress response [17].

2.2. Performance of mortar cubes treated with live and UV-killed *Gloe.* PCC73106 (experiments A)

2.2.1. Preparation of the mortar cubes

Mortar cubes of a size of 50 × 50 × 50 mm were prepared according to ASTM C109/C109M-13, the international standard test method for compressive strength of hydraulic cement mortars, and were demolded after 24 h. The mortar mixture had the following composition (per 12 cubes): 1060 g cement, 2915 g sand and 514 ml water. The mortar cubes were cured for 28 days under humid atmosphere (90% R.H., 20 °C) prior to the treatment of bacteria. After curing, the mortar cubes weighed 288.5 ± 3.7 g.

2.2.2. Experiments with live and killed *Gloe.* PCC73106 on the mortars

The mortar cubes were separated into 5 groups, each group with 6 cubes. The first and second groups were treated with freshly

washed cells, the third group was treated with UV-killed cells, and the fourth and the fifth groups were not treated with cells. During the cell treatment, mortar cubes were immersed in the cell solution (with a concentration of 3.5 × 10⁷ cells/ml) for half an hour, allowing the cells to attach to the mortar surfaces. After the treatment, the first four groups of mortar cubes were immersed in a 100 ml solution composed of calcium chloride (290 mM) and sodium bicarbonate (200 mM) for 7 days. The concentration of calcium chloride is within the range of other studies of MCP for mortar or concrete restoration [8,18,19]. Among them, the second group was covered with a black plastic to inhibit photosynthetic activities, and the others were exposed to a light intensity of 20 μE m⁻² s⁻¹ for 12 h, and kept under darkness for 12 h. The fifth group was immersed in deionized water, and served as the control. At the end of the experiment, the mortar cubes were dried in the oven at 78 °C for 24 h and the typical mortar characteristics were monitored, including compressive strength and water absorption tests. In this experiment, a duration of 7 days was chosen instead of 28 days in order to compare the results for live and UV-killed cells. All tests were conducted in triplicates.

2.2.3. Performance tests

The weight of the mortar cubes was measured before and after the experiment. Before the experiment, the cubes were oven-dried at 78 °C for 24 h and the weight of each cube was recorded individually as W_1 . The temperature was maintained at 78 °C rather than 105 °C, according to EN 1097-6 standard (tests for mechanical and physical properties of aggregates), to avoid the removal of inter-packet water from hydrated calcium silicates, which generally occurs at 78 °C to 90 °C [20]. After the treatment, cubes were again oven-dried at 78 °C for 24 h and the weight of each cube was recorded as W_2 . The weight change of the treated mortar cubes is calculated as $W_2 - W_1$.

The weight of the precipitates formed in the bulk solution was measured in the following procedure. After shaking, the bulk solution with a volume of 50 ml was filtered through 0.45 μm membrane filter, and the filter was oven-dried at 78 °C for 24 h. The weight of the filter was recorded as W_3 , and the weight of the precipitates on the filters was recorded as W_4 . The weight of the precipitates in the bulk solution is therefore $(W_4 - W_3) \times (V/50)$, in which V denotes the volume of the total bulk solution (ml).

Compressive strength tests were done according to ASTM C109/C109M-13 using a FORNEY FT-40 compression tester. All the tested cubes were placed in the same orientation to avoid the error due to varied strength in different directions.

To determine the increase of resistance toward water penetration on the treated samples, a water absorption test was performed based on RILEM Test Method II.4. The four sides of the mortar cubes were affixed with tape to prevent water penetration through them. The mortar cubes were then exposed to water with a racket underneath. At regular time intervals, 15 min, 30 min, and 1, 1.5, 3, 5, 8, 24, 48, 72, 96, 120, 144 and 168 h [18], they were removed from the water and immediately weighed after removing the excess water on the surface with a damp towel.

The porosity and the pore size distribution of the mortar cubes were measured by an automatic mercury porosimeter (Micromeritics AutoPore IV 9500, USA). Prisms with a size of 5 × 5 × 10 mm were cut from one corner of the mortar cubes and prepared for the mercury intrusion tests. Prior to the measurement, the samples were placed in a penetrometer (model: 07-0569) and dried under vacuum at 78 °C for 6 h to drive off any physical-sorbed water and volatile organic matters. The low mercury-filling pressure was at 1.50 psia, and the pressure was increased incrementally to an ultimate pressure up to 60,000 psia. The equilibration time in the measurements was 30 s to ensure fully equilibrated porosimetry curves.

The significance of difference among the treatments under different conditions was measured using one-way ANOVA analysis. The weight changes of mortar and precipitates, the compressive strength, and the water absorption at 168 h were analyzed.

2.3. Microbial calcification on the mortar cubes (experiments B)

2.3.1. Preparation of the mortar cubes

Cubes with a size of $30 \times 30 \times 15$ mm were prepared in an aluminum mold. Before the experiment, each cube was cut with a diamond saw into 8 pieces, with a dimension of $15 \times 15 \times 6$ mm to fit the analytical instruments. Isopropyl alcohol served as the cutting agent to moisturize and cool down the saw. The cubes were then washed with acetone in an ultrasonic cleaner for 5 min. The surface of the mortar was sterilized by being exposed to the UV light for 1 h just before the experiments.

2.3.2. Biofilm-treating experiments

Each mortar cube was exposed to the UV light for 1 h, and then immersed in the cell suspension (2×10^9 cells/ml), allowing cells to attach to the mortar. After being treated with cells for half an hour, the mortar cubes were removed and immersed in the experimental solution. The experiments were performed in 150 ml flasks with 31 ml solution comprised of CaCl_2 and NaHCO_3 with a concentration of 290 mM and 0.4 mM, respectively. All flasks were previously autoclaved at 121°C for 20 min. Both the calcium chloride solution and the NaHCO_3 solution were filtered through the $0.2 \mu\text{m}$ polycarbonate membrane filter to be sterilized. The saturation index was calculated by PHREEQC, and determined to be $\Omega_{\text{aragonite}} 1.7$ and $\Omega_{\text{calcite}} 2.5$ for aragonite and calcite. The experimental setup was an open system that was equilibrated with the synthetic atmosphere. The flasks were constantly shaken at a speed of 60 rpm for 7 days. At the beginning and the end of the experiments, pH was measured by Mettler Toledo pH meter. A 5 ml experimental solution was filtered through the $0.45 \mu\text{m}$ cellulose acetate membrane filter to analyze the dissolved Ca^{2+} concentration by an iCE 3500 atomic absorption spectroscopy (ThermoFisher, USA) equipped with a deuterium lamp.

At the end of the experiment, the mortar cubes were removed from the solution and washed with deionized water twice, followed by air drying. All the experiments were conducted in duplicates. Sterility was ensured throughout the experiments by using sterile pipettes, flasks and solution in a biosafety cabinet.

2.3.3. Attachment of the cells to the mortar cubes

Separate experiments C, without adding bicarbonate, were conducted to examine the attachment of the bacteria to the mortar cubes. All the procedures were the same as the steps above, except for adding the bicarbonate to the bulk solution. After 1 day of shaking at a speed of 60 rpm, the mortar cubes were removed from the solution and washed with deionized water twice. Following air drying, samples were vacuum-dried in a sputter coater for more than 2 h. Scanning electron microscope (SEM) images were taken to investigate the attachment of the cells.

2.4. Characterization of the treated mortar surfaces

2.4.1. Scanning electron microscopic observation and energy-dispersive spectroscopic measurement

Morphologies of cells, biofilms and precipitates were observed under a Zeiss GEMINI SUPRA 55 Field Emission Scanning Electron Microscope (FE-SEM), coupled with an Oxford X-Max^N 150 Energy Dispersive Spectroscopy (EDS) at the School of Earth Sciences and Engineering at Nanjing University. Samples for FE-SEM observation were gold sputtered. A beam potential of 1–5 kV was used for the morphological observation, and 20 kV was applied for EDS analyses. To survey the percentage of precipitates in different morphologies, five random SEM images of a total area larger than $12,500 \mu\text{m}^2$ were taken, and the precipitates in each morphology were counted.

2.4.2. Raman spectroscopy analyses

Raman spectroscopy analyses for samples were carried out under the NTEGRA Spectra system from NT-MDT (Russia) equipped with an upright optical microscope. Raman spectra were acquired at 532 nm laser wavelength with 600 grooves per mm grating. An accumulation number of 300 over an acquiring period of 0.5 s was adopted for all of the spectra.

3. Results and discussion

3.1. Changes in properties of the mortar cubes

3.1.1. Weight change of the mortar cubes

Over the 7-day experimental period in experiments A, there was no weight gain of the control cubes and the cubes with bacteria alone, while the weight gain of the abiotic cubes was around $0.315 \pm 0.007\%$ (Table 1). Therefore, the absorption of cells to the mortar cubes did not result in the weight change. The weight gain of the mortar cubes treated with live cells was the highest among all the treatments (Table 1), while that of cubes treated with UV-killed cells or live cells under darkness was slightly higher than that of the abiotically treated cubes. The ANOVA analysis on the weight change of mortars treated abiotically, with live cells under illumination and darkness, and with UV-killed cells showed that the p value is less than 0.05 (Table 2), indicating that the difference among them is significant. It showed the significant difference between mortars treated with live cells and UV-killed cells as well.

The weight of the precipitates collected from the bulk solution in experiments A for the control was 0, while the precipitates collected from the other four conditions were more than 0.3400 g (Table 1). The ANOVA analysis on the weight of precipitates under these four conditions showed that the p value is higher than 0.05 (Table 2), indicating that the difference among them is not significant.

3.1.2. Compressive strength of the treated mortar cubes

At the end of experiments A, the compressive strength of the mortar cubes treated with UV-killed cells increased, while that of the abiotically treated cubes decreased. There was no significant difference between the mortar cubes treated with live cells under illumination and darkness, and both are comparable to that of the control. The compressive strength of the control at the seventh day

Table 1
Weight change of the mortar cubes and the precipitates in the bulk solution.

Experimental groups	Control	Abiotic	Live cells under illumination	Live cells under darkness	UV-killed cells
Weight change of mortar cubes (%)	0	0.315 ± 0.007	0.380 ± 0.000	0.337 ± 0.023	0.333 ± 0.006
Weight of the precipitates (g)	0	0.324 ± 0.015	0.342 ± 0.023	0.348 ± 0.022	0.344 ± 0.024

Table 2
ANOVA analysis of weight change, compressive strength and water absorption under different conditions.

	Five conditions including control		Four conditions excluding control		Between UV-killed cells and live cells	
	F Value	p	F Value	p	F Value	p
Weight change of mortar	540.80	<0.0001	11.97	0.0038	196	0.0002
Weight of precipitates	139.75	<0.0001	3.10	0.0512	0.47	0.5078
Compressive strength	10.46	0.0013	11.10	0.0032	8.97	0.0401
Water absorption, 168 h	19.06	0.0001	5.95	0.0196	22.56	0.0090

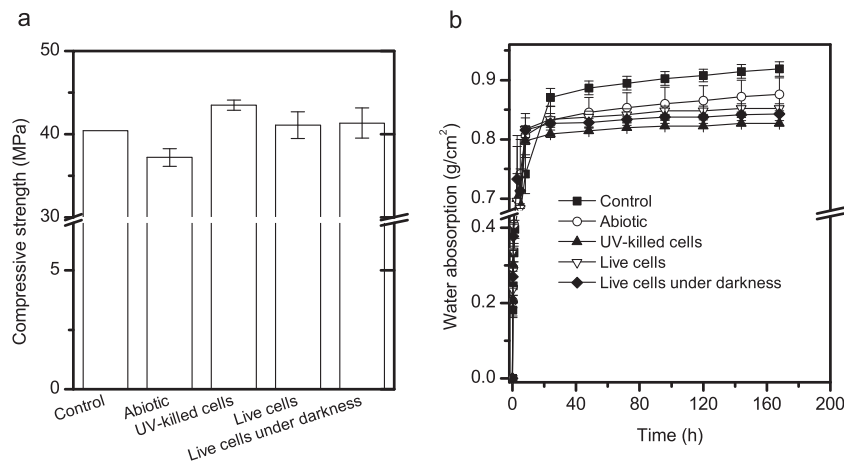


Fig. 1. The compressive strength (a) and water absorption (b) of the mortar cubes under different conditions for 7 days.

was 40.4 MPa, that of the mortar cubes treated with UV-killed cells was 43.5 ± 0.6 MPa, and that of the abiotically treated cubes was 37.2 ± 1.1 MPa (Fig. 1a). The UV-killed cells increased the compressive strength of the mortar cubes by 7.7% in 7 days. By comparison, the compressive strength of the abiotically treated cubes decreased by 7.9% over the same period. The ANOVA analysis showed that the difference among the treatments under 5 conditions is significant (Table 2).

3.1.3. Water absorption

Compared to the control, all the treatments in experiments A decreased the water absorption. Among them, the mortar cubes treated with UV-killed cells had the lowest water absorption (Fig. 1b). By the end of the water absorption test, UV-killed cells decreased the water absorption by 10.0%, whereas the abiotically treated cubes decreased it by 4.7%. Live cells under illumination and darkness decreased the water absorption of mortar cubes by 7.3% and 8.3%, respectively. Compared to all other conditions, the control took a longer time to reach the plateau. The ANOVA analysis of the water absorption at 168 h under different conditions showed that the difference is significant (Table 2).

3.1.4. Porosity and pore size distribution

After the 7-day experiments, the porosity of the control mortar cubes was 16.9%, and that of the cubes treated with live cells under illumination, live cells under darkness, and UV-killed cells was 14.5%, 14.2% and 12.7%, respectively. According to the log differential intrusion versus pore size, the most widely distributed pore size within the control mortar cubes was 50.4 nm, while in cubes treated with live cells under illumination and under darkness was 40.3 nm, and in cubes treated with UV-killed cells was as narrow as 26.3 nm (Fig. 2). In addition, the control showed abundant large pores with diameters larger than 70 μm , which disappeared in the microbially treated samples (Fig. 2).

3.1.5. Performance of the treatments

For the treated mortars, different weight gains and a similar amount of deposits filtered from the bulk solution can be attributed to the difference in treatments. The highest weight gain were observed in the treatment with live cells under illumination. The weight increase of mortar cubes treated with UV-killed/live cells in our experiments is comparable to the microbial carbonate precipitation in recycled concrete aggregates [19], in which 454 mM calcium chloride and 353 mM carbon source was used, and a 0.345% weight gain was reached over a 3-day period. In another 3-day experiment [21] with urea (167 mM) and sodium bicarbonate (25 mM) as carbon sources, and calcium chloride at 225 mM, the weight increase of mortar cubes with a dimension of $100 \times 100 \times 100$ mm was around 65–77 mg. The weight gain of the mortars in our experiments with different treating methods was similar to or higher than that in other studies.

Cells and their excreted organic matter filled the pores and induced carbonate precipitates, which altered the surface wettability, compressive strength [22], porosity and pore size distribution of the mortars. In our study, bacterial cells and extracellular substances built a physical-chemical barrier to hinder the movement of water [23] and affected its capacity of absorbing water. The UV-killed cells produced more organic matter than live cells; therefore the specimens presented less water absorption, which is in good agreement with the reported data in previous studies using heterotrophic microbes [21]. A comparable 13–21% decrease in water absorption was observed in recycled concrete aggregates after biodeposition [20]. The higher percentage in the latter study might be due to urea, which can be hydrolyzed by heterotrophs to continuously produce CO_2 or bicarbonate, resulting in a more homogeneous precipitation layer. The increase in compressive strength improved by UV-killed cells is comparable to other experiments with live heterotrophic bacteria *S. pasteurii* [18,24]. The treatment with *Shewanella* after 7 days showed an increase of

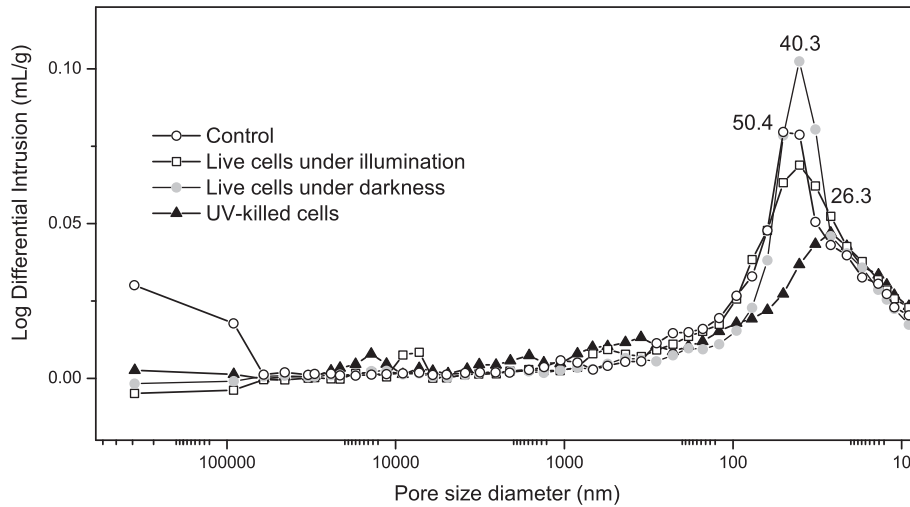


Fig. 2. The pore size distribution of the mortar cubes obtained by mercury intrusion measurements.

compressive strength up to 15% [25]. With *Acinetobacter johnsonii*, the compressive strength is 6% higher than the control after 7 days, and 21% higher after 28 days [26]. In our experiment, the compressive strength of the abiotically treated mortars decreased as a result of the deleterious effect of calcium chloride [27], whereas no decrease was observed in the compressive strength of mortar cubes treated with live cells, indicating an improvement was achieved compared to abiotically treated cubes. It is worthy to note that our experiments were done only in a 7-day timeframe, and the compressive strength was expected to be much higher after a longer treatment.

Although the mortar cubes treated with live cells showed the highest weight gain, they did not present the best performance in the compressive strength, water absorption and mercury intrusion tests. In comparison, the UV-killed cells produced more EPS while being exposed to the UV-light, which greatly decreased the porosity, and contributed to the best performance in water adsorption and compressive strength.

3.2. Mechanism of carbonate precipitation

3.2.1. Dynamics of the bulk solution

In experiments B, the changes in pH and calcium concentration did not show significant difference under four conditions. Initially,

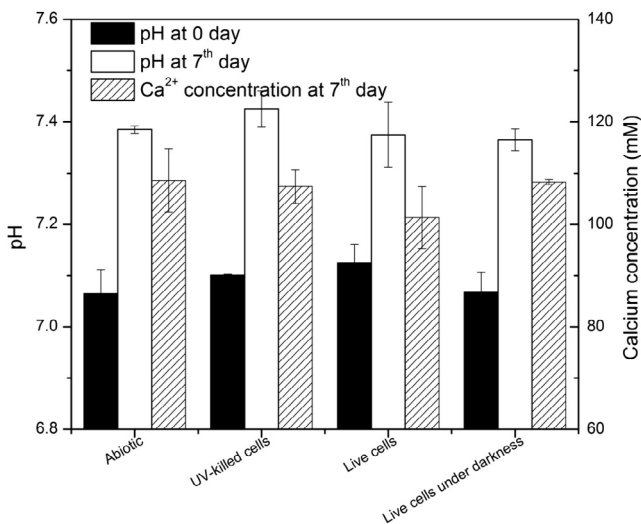


Fig. 3. The pH and calcium concentration dynamics of the bulk solution.

the pH of all the samples was at 7.1, and it increased to 7.4 after 7 days (Fig. 3). This increase can be a result of the dissolution and/or hydration of the mortar that released OH^- into the solution [28]. The initial calcium concentration for all conditions was 290 mM, and after 7 days it decreased to 109 ± 6 mM under the abiotic condition, 107 ± 3 mM after being treated with UV-killed cells, 101 ± 6 mM after being treated with live cells under illumination, and 108 ± 1 mM after being treated with live cells under darkness.

Thus, the difference in the performance of different treatments lies only in the cell-adhered areas in mortar cubes. Mortars treated with UV-killed cells, live cells under illumination and live cells under darkness were covered with a biofilm consisted of dead cells with a thicker EPS layer, metabolically active cells with a thinner EPS layer, and photosynthesis-disabled cells, respectively. The fact that the bulk solution was the same, while the mortar cubes treated differently showed significant differences supports the conclusion we drew before that the biofilms strongly impacted the microenvironment around the mortar cubes.

3.2.2. Attachment of bacteria to the mortar cubes

After half an hour of exposure to the bacteria solution in experiments C, the mortar cubes were washed gently with sterile deionized water to remove dangling bacteria. They were transferred to a calcium chloride solution, and the cells remained covering the mortar surface after being shaken for 1 day. Most of the cells attached to the defective or rough surfaces of the mortar cubes. A thin layer of EPS around live cells (Fig. 4a) linked cells and helped them to attach to the surface of the mortar (Fig. 4b). All the EPS around live cells were found between the cells and the mortar surface. In comparison, a larger coverage by bacteria was observed in the presence of UV-killed cells than live cells. After being exposed to UV light, the cells produced more EPS (Fig. 4), a thicker layer of EPS not only resided between the UV-killed cells and the mortar surface but also curled up to envelop the cells (Fig. 4c, d), which is in agreement with other studies [17].

3.2.3. Carbonate precipitation on the mortar surface under the abiotic condition

Different from the original mortar surface (Fig. 5a), after being immersed in the bulk solution for 7 days in experiments B, the mortar surfaces under the abiotic condition were incompletely covered with calcium carbonates (Fig. 5b, c). Unlike microbially formed carbonates, they were loosely attached to the substrate surface in the abiotic condition, and was easily removed by sonica-

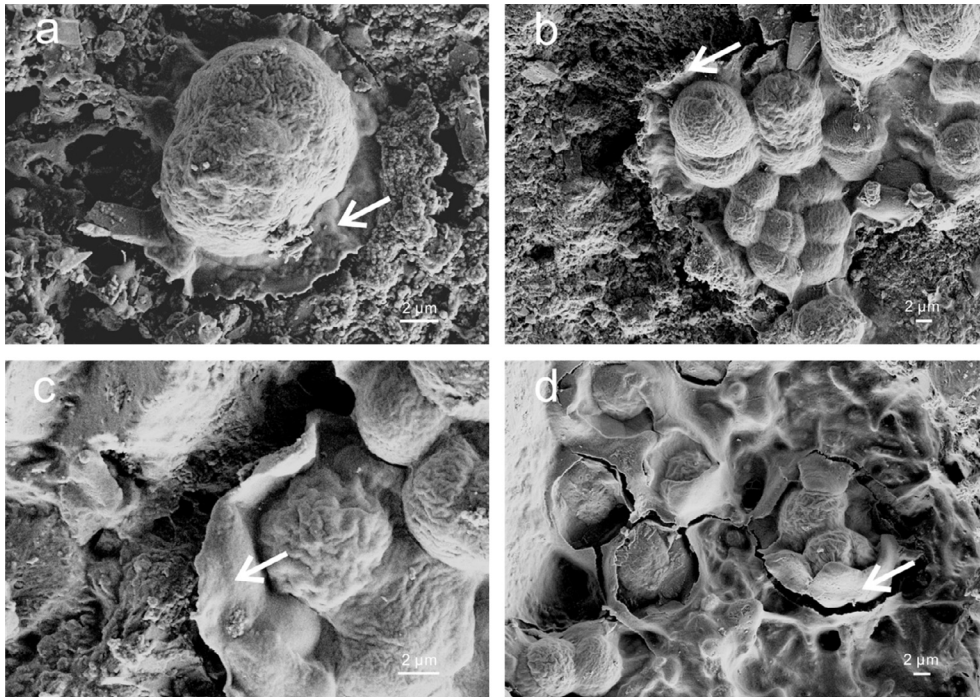


Fig. 4. EPS of live and UV-killed cells. A thin layer of EPS around live cells (a). The EPS layer resided between the cells and the mortar surface (b). A thicker layer of EPS around UV-killed cells (c). The EPS layer curled up and enveloped the cells (d).

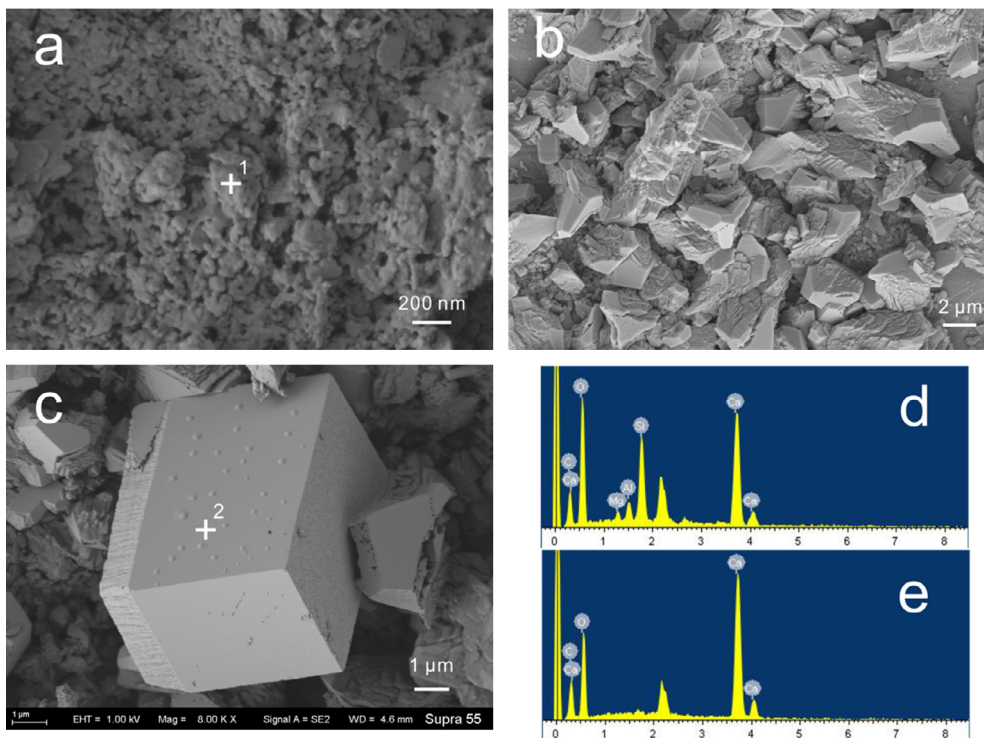


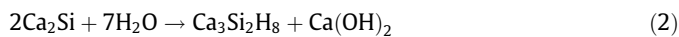
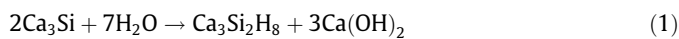
Fig. 5. SEM images and EDS analysis of the mortar surface treated abiotically. The cement from the original mortar surface was exposed (a). The irregular-shaped carbonate precipitates deposited on the mortar surface (b). A big rhombohedral calcite with “bubbles” on the crystal surface and a bloom tail (c). The EDS spectra corresponds to point 1, indicating calcium silicates (d). The EDS spectra corresponds to point 2, representing calcium carbonate (e).

tion [10]. The EDS analysis at point 1 showed the components made up of Ca, Si, O and Al (Fig. 5d), which are typical elements of the calcium silicates hydrate and calcium aluminate [29]. Counting 564 precipitated grains on a total area of $12500 \mu\text{m}^2$, a majority (536 grains) of the precipitates on the mortar surface under the

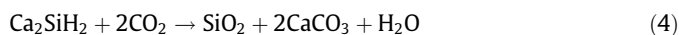
abiotic condition were in an irregular shape, with 2–3 μm in length and 1.5 μm in width (Fig. 5b). All of them had smooth surfaces on the one side and a step-like structure on the other. Rhombohedral carbonates with a size of around 5 μm were observed as well (Fig. 5c), accounting for approximately 5% of all the precipitates.

Differentiated from the common rhombohedra, these precipitates showed “bubbles” on one side of the crystal face and had a “bloom tail” beside it. The EDS analysis on the point 2 showed the peaks of Ca, C and O, revealing this precipitate to be calcium carbonate (Fig. 5e). Furthermore, the Raman spectra of these calcium carbonates showing the peaks at 284, 472, 711 and 1084 cm^{-1} confirms the carbonates to be calcite (Fig. 6).

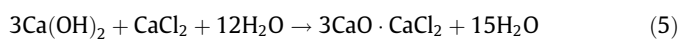
The investigated interface is immersed in the bulk solution consisted of a high concentration of calcium chloride and a low concentration of sodium bicarbonate. The precipitation behavior on the mortar surface was impacted not only by the saturation state of the bulk solution but also by the composition of the mortar. The hydration of calcium silicates (reaction 1 and 2) is the most active within 14 days after the cement meets with water, and continues moderately over time [30]. The cement hydration leads to the production of $\text{Ca}(\text{OH})_2$, resulting in a higher alkalinity surrounding the mortar surface [28].



where Ca_3Si is tricalcium silicate, $\text{Ca}_3\text{Si}_2\text{H}_8$ represents tricalcium silicate hydrate, Ca_2Si is bicalcium silicate, $\text{Ca}_2\text{Si}_2\text{H}_8$ represents bicalcium silicate hydrates, and $\text{Ca}(\text{OH})_2$ stands for calcium hydroxide. In addition, with the penetration of CO_2 from the atmosphere, reactions 3 and 4 on the mortar surfaces can occur [27], thus forming calcium carbonate on the mortar surface,



However, due to the polymerization of the silicate chains in Ca_2SiH_2 (bicalcium silicate hydrate) in the presence of CO_2 , the mortar decreases the volume and shrinkage, thus causing cracks [31]. As a de-icing salt, calcium chloride causes deleterious effects on mortar through reaction 5 [27],



Therefore, $\text{Ca}(\text{OH})_2$, dicalcium silicate (Ca_2Si) and tricalcium silicate (Ca_3Si) are consumed, and CaO , CaCO_3 and SiO_2 are produced in these processes [27]. In this study, the calcium carbonate on the mortar surface under the abiotic condition is a result of both the carbonation and the oversaturation due to the high pH microenvironment around the mortar surface. The high concentration of CaCl_2 in the bulk solution contributed to a large amount of free Ca^{2+} ions,

and the initial bicarbonate resulted in the oversaturation of calcium carbonate as calculated by PHREEQC. In the process of calcium carbonate precipitation, bicarbonates were consumed, and then CO_2 available from the atmosphere was constantly dissolved into the solution, leading to a further precipitation. This process limited reaction 4 to occur by consuming the available bicarbonate or carbonate in the solution, thus protecting the mortar from shrinking.

3.2.4. Carbonate precipitation on the mortar surface treated with live cells

Photosynthesis of cyanobacteria contributed to the carbonate precipitation by increasing the pH in the microenvironment. The calcification of live cells might have contributed to the highest weight gain of mortars treated with live cells under illumination (Table 1). The mortar cubes treated with live cells prior to being exposed to the bulk solution in experiments B showed a completely different appearance from that of the abiotic condition after the 7-day interaction (Fig. 7). The biofilm surface was highly calcified and exhibited rough, fissured and wrinkled features (Fig. 7a, b). The morphology of round and smooth cells could no longer be identified as they were. The calcified biofilm (Fig. 7a, b) and cell remnants (Fig. 7c) largely covered the mortar surface. Above the biofilm, irregular-shaped precipitates scattered and showed similar linear cracks along the same direction (Fig. 7b, in the white ellipses). The round-shaped calcified cells always appeared in pairs and on top of them formed “star-shaped” calcium carbonates with a size of 3 μm . While all of the cells and the EPS were calcified, most of the trapezoidal prism calcite grew from the cell surfaces (Fig. 7c). The point was always stretching from the center of the spherical cell remnant. The morphology of precipitates varied at different sites on the same mortar surface (Fig. 7). Some of the crystals were smaller (Fig. 7c), while some were much larger and stacked (Fig. 7d). Besides, much larger precipitates with a size of about 10 μm presented where the cell morphology was no longer recognizable. These precipitates were like twin crystals, with 3 rectangular prisms crossing at the center at a 90-degree angle. Each of the precipitates had at least one face of the crystal intensively ditched. The compositions were all confirmed by EDS and Raman spectra (Fig. 6) to be calcite. The irregular shape of crystals is strongly influenced by numerous factors, such as small molecular additives (inorganic ions, small molecular organic species and solvents), soluble and insoluble biomacromolecules, the ratio of the functional groups to the calcium concentration, and temperature [32,33]. In addition, the metabolic activity of live cells led to further changes around mortar surfaces. For example, live cyanobacteria produced calcifying macromolecules, providing more nucleation sites [34].

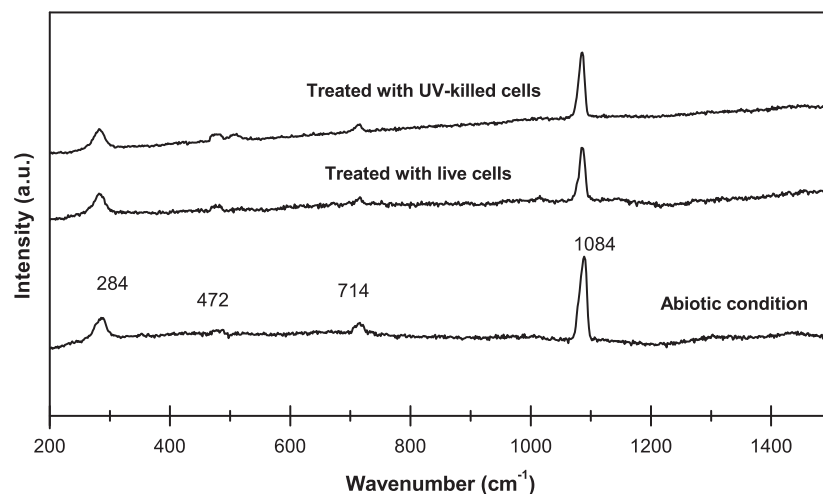


Fig. 6. Raman spectra of the precipitates from different conditions showing them all to be calcite.

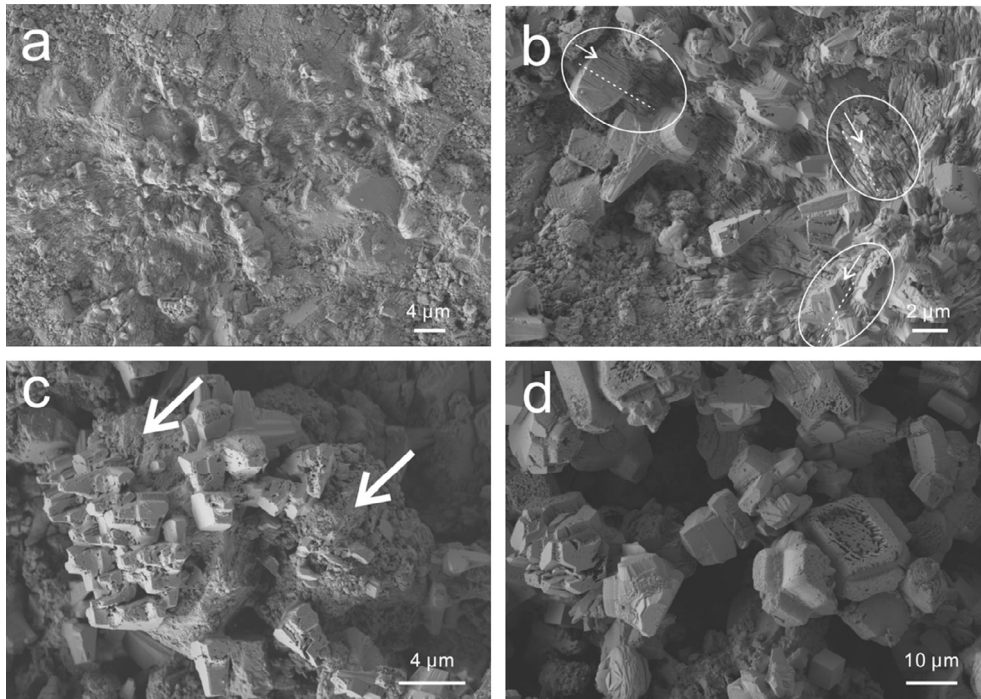


Fig. 7. SEM images of the mortar surface treated with live cells. The biofilm was highly calcified and exhibited rough, cracked and wrinkled features (a). Irregular-shaped precipitates scattered and showed similar linear cracks along the same direction as the biofilm underneath (b). The trapezoidal prism calcite grew from the cell surface (c, the white arrow points to the cell remnant). Bigger twin crystals buried the biofilm (d).

3.2.5. Carbonate precipitation on the mortar surface treated with UV-killed cells

Compared to live cells in experiments B, UV-killed cells were less calcified (Fig. 8). The thin and smooth UV-killed biofilm covering the surface of the mortar was still obvious (Fig. 8a). On top of that, the orthorhombic and rhombohedral calcites with sizes

ranging from 4 to 10 μm were randomly sitting on the biofilm or attached to the cell surface. The Raman spectra of the rhombohedral precipitates confirm them to be calcites (Fig. 6). Few spherical vaterite presented close to the calcite as well (Fig. 8a, white arrow). Due to the high vacuum in the SEM chamber, the interface of the newly formed calcite and the biofilm/cell surface separated

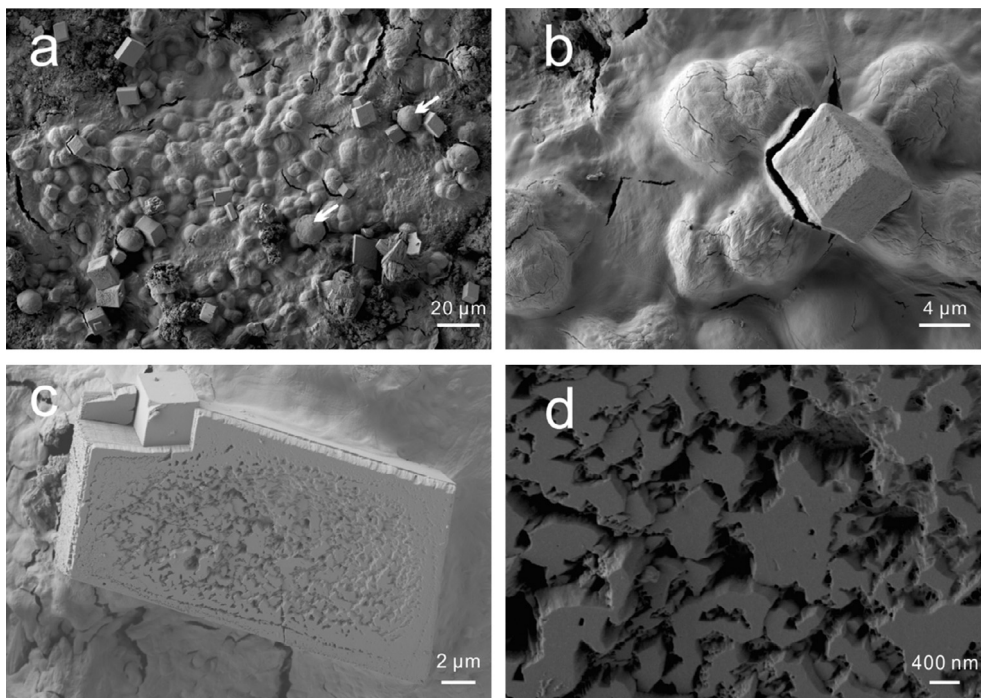


Fig. 8. SEM images of the mortar surface treated with UV-killed cells. A thin and smooth biofilm covering the surface of the mortar, and on top of that residing a few rhombohedral calcites and spherical vaterite (a, the white arrow points to vaterite). The interface of the cells and the precipitated calcite, and the separation between them were due to the vacuum effect (b). A large rhombohedral crystal with a porous surface was observed, and two smaller crystals that developed beside it in the same direction were without pores (c). An enlarged area from the large crystal (c) showed more details of the pitches (d).

(Fig. 8b). Unlike the calcites formed with the mediation of live cells that were composed of linear cracks, the calcites were intact and in a perfect rhombohedral crystal shape. In some cases, large rhombohedra elongated in one direction with a length of around 10 μm and a width of 5 μm were observed (Fig. 8c). On the larger crystals, the pitches on the crystal surfaces were presented. More details of these pitch patterns are shown in Fig. 8d. Nevertheless, smaller and intact rhombohedral crystals growing beside the big crystal were in the same orientation (Fig. 8c).

The EDS mapping of the mortar surface partially covered by the UV-killed biofilm was obtained (Fig. 9). The distribution of the element calcium can obviously be discerned among the newly formed precipitate, mortar surface and biofilm, in the order from the highest concentration to the lowest. The carbon signal was much higher on the biofilm than on the precipitates or uncovered mortar surface. Although a trace amount of silicon can be observed on the biofilm, the majority was from the mortar surface where calcium silicate hydrant and silica were located. The counts of magnesium were mainly on the mortar surface without the biofilm, and were

not evenly distributed. Several patches of sulfur were observed on the mortar surface and around the edges of the biofilm.

UV-killed cells were not metabolically active; therefore, cell surfaces and EPS were mainly responsible for their impact. EPS have been shown to protect cells against dehydration and UV radiation, to prevent them from detrimental biomineralization, and aid the biofilm attachment [35,36]. The adhesion of cells to the hard substrate depends on several parameters, including substrate composition, pH, organic film, cell density and surface roughness [37]. In this study, the EPS promoted the *Gloe.* PCC73106 adhering to the rough mortar surface, and subsequently formed calcium carbonate above them by attracting the positively charged Ca^{2+} using the negatively charged functional groups, such as carboxylate, amine, phosphoryl/phosphodiester and hydroxyl, on the cell surface and EPS [38]. As a consequence, the biofilm served as a primer for the carbonate coating [21]. Not only of cyanobacteria, but also of heterotrophs, EPS were found to enhance the carbonate precipitation [39]. Some of the rhombohedral precipitates were closely attached to the cells, while the others were randomly scattered

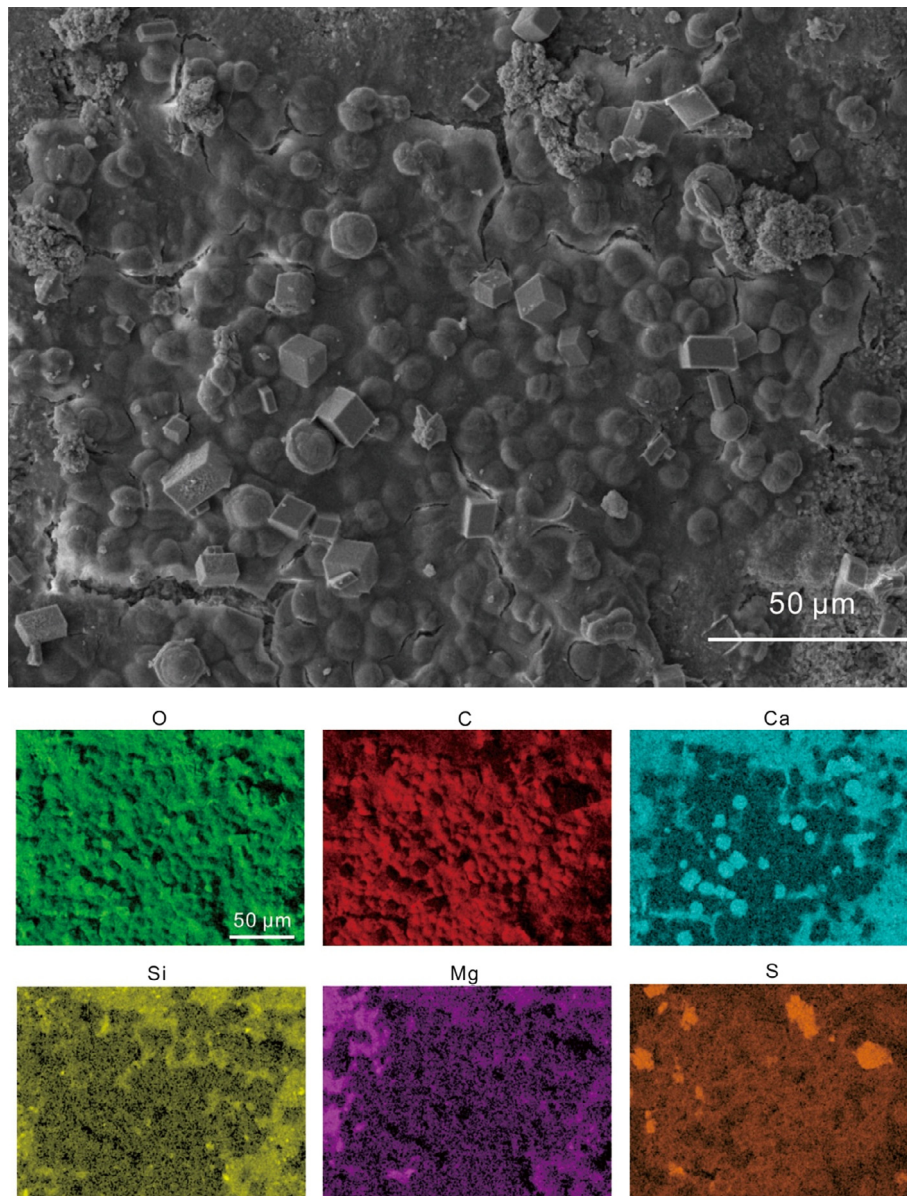


Fig. 9. Elemental mappings of the mortar surface partly covered with the biofilm. The elements of oxygen, carbon, calcium, silicon, magnesium and sulfate were collected. The higher counts of the color pixels indicate a higher content of that element.

on the biofilm. In contrast to live cells, UV-killed cells were not entirely calcified due to a thicker EPS layer on *Gloe. PCC73106*. The pores occurred in big crystals rather than in small precipitates possibly due to the incorporation of the organic matter, as revealed in an experiment to synthesize a single calcite crystal with a porous surface by the templating of polymer latex particles with functional groups of $-\text{CO}_2^-$, $-\text{SO}_3^-$, $-\text{PO}_3^{2-}$, and quaternary ammonium surface [33]. No rhombohedral calcite was observed beyond the biofilm, indicating that all of these rhombohedral crystals were closely associated with UV-killed cells or EPS.

4. Conclusions

This study investigated the carbonate precipitation in the mortars treated with live and UV-killed *Gloe. PCC73106*. Based on the following summary, this study provided the first evidence that cyanobacteria *Gloe. PCC73106*, especially UV-killed cells, are suitable for improving the performance of mortar.

- (1) Compared to UV-killed cells, live cells led to a higher amount of carbonate precipitation on the mortar cubes.
- (2) Mortar cubes treated with UV-killed cells achieved the highest durability by increasing the compressive strength, and decreasing the water absorption as well as the porosity.
- (3) The EPS enhanced biofilm formation on the mortar cubes and, subsequently, triggered carbonate precipitation on the biofilm. In addition, a thicker EPS protected cells from being calcified.

In contrast to other experimental approaches, the novelty of this study lies in the usage of a simple and cheap chemical solution and autotrophic cyanobacteria. The calcium chloride solution mixed with sodium bicarbonate without any other additional ions helps to overcome the obstacle of using medium, where presence of Mg^{2+} , SO_4^{2-} and PO_4^{3-} can inhibit the precipitation process of calcium carbonate [40]. Furthermore, the suggested technological development not only excludes possible influences from other chemicals, but also lowers the cost of the experiments as well as the subsequent potential application.

Acknowledgements

This work was supported by the National Science Engineering Research Council Canadian (Grant number 354741), the Canadian Foundation for Innovation (project number 24591), and the Ontario Research Fund of Ministry of Research and Innovation (project number 24591) to Maria Dittrich, the National Natural Science Foundation of China (Grant number 41425009) to Xiancai Lu, and the Ontario Trillium Scholarship to Tingting Zhu. We thank Prof. Muhammed Merroun for his generous support at the microscope center at University of Granada during the preliminary research for this study. We thank Xinchu Jia at Nanjing University for the help with mercury intrusion porosimetry. We appreciate the help of Prof. Karl Peterson and his PhD student Haizhu Lu at University of Toronto for the mortar preparation and the measurements of compressive strength. We are grateful to Four anonymous reviewers for their constructive comments and to Jennifer Krissilas and Sheryl Stevenson for their editorial proofreading.

References

- [1] V. Achal, A. Mukherjee, D. Kumari, Q. Zhang, Biomineralization for sustainable construction—a review of processes and applications, *Earth Sci. Rev.* 148 (2015) 1–17.
- [2] T. Zhu, M. Dittrich, Carbonate precipitation through microbial activities in natural environment, and their potential in biotechnology: a review, *Front. Bioeng. Biotechnol.* 4 (2016).
- [3] J. McCutcheon, I.M. Power, A.L. Harrison, G.M. Dipple, G. Southam, A greenhouse-scale photosynthetic microbial bioreactor for carbon sequestration in magnesium carbonate minerals, *Environ. Sci. Technol.* 48 (2014) 9142–9151.
- [4] A.J. Phillips, R. Gerlach, E. Lauchnor, A.C. Mitchell, A.B. Cunningham, L. Spangler, Engineered applications of ureolytic biomineralization: a review, *Biofouling* 29 (2013) 715–733.
- [5] V. Stabnikov, V. Ivanov, J. Chu, Construction biotechnology: a new area of biotechnological research and applications, *World J. Microbiol. Biotechnol.* 31 (2015) 1303–1314.
- [6] S.S. Bang, J.K. Galinat, V. Ramakrishnan, Calcite precipitation induced by polyurethane-immobilized *Bacillus pasteurii*, *Enzyme Microb. Technol.* 28 (2001) 404–409.
- [7] V. Achal, A. Mukherjee, S. Goyal, M.S. Reddy, Corrosion prevention of reinforced concrete with microbial calcite precipitation, *ACI Mater. J.* 109 (2012) 157–163.
- [8] W. De Muynck, K. Cox, N. De Belie, W. Verstraete, Bacterial carbonate precipitation as an alternative surface treatment for concrete, *Constr. Build. Mater.* 22 (2008) 875–885.
- [9] N.K. Dhami, M.S. Reddy, A. Mukherjee, Biomineralization of calcium carbonates and their engineered applications: a review, *Front. Microbiol.* 4 (2013).
- [10] T. Zhu, C. Paulo, M.L. Merroun, M. Dittrich, Potential application of biomineralization by *Synechococcus* PCC8806 for concrete restoration, *Ecol. Eng.* 82 (2015) 459–468.
- [11] T. Toncheva-Panova, I. Pouneva, G. Chernev, K. Minkova, Incorporation of *synechocystis salina* in hybrid matrices. Effect of UV-B radiation on the copper and cadmium biosorption, *Biotechnol. Biotechnol. Equip.* 24 (2010) 1946–1949.
- [12] M. Obst, B. Wehrli, M. Dittrich, CaCO_3 nucleation by cyanobacteria: laboratory evidence for a passive, surface-induced mechanism, *Geobiology* 7 (2009) 324–347.
- [13] H.S. Chafetz, C. Buczynski, Bacterially induced lithification of microbial mats, *Palaios* (1992) 277–293.
- [14] M.F. Macedo, A.Z. Miller, A. Dionísio, C. Saiz-Jimenez, Biodiversity of cyanobacteria and green algae on monuments in the Mediterranean Basin: an overview, *Microbiology* 155 (2009) 3476–3490.
- [15] R. Rippka, Isolation and purification of cyanobacteria, *Methods Enzymol.* 167 (1988) 3–27.
- [16] I.A. Bundeleva, L.S. Shirokova, O.S. Pokrovsky, P. Bénézeth, B. Ménez, E. Gérard, S. Balor, Experimental modeling of calcium carbonate precipitation by cyanobacterium *Gloeocapsa* sp., *Chem. Geol.* 374–375 (2014) 44–60.
- [17] M. Ehling-Schulz, W. Bilger, S. Scherer, UV-B-induced synthesis of photoprotective pigments and extracellular polysaccharides in the terrestrial cyanobacterium *Nostoc commune*, *J. Bacteriol.* 179 (1997) 1940–1945.
- [18] V. Achal, A. Mukherjee, M.S. Reddy, Microbial concrete: way to enhance the durability of building structures, *J. Mater. Civil Eng.* 23 (2011) 730–734.
- [19] J. Qiu, D.Q.S. Tng, E.-H. Yang, Surface treatment of recycled concrete aggregates through microbial carbonate precipitation, *Constr. Build. Mater.* 57 (2014) 144–150.
- [20] A.M. Grabiec, J. Klama, D. Zawal, D. Krupa, Modification of recycled concrete aggregate by calcium carbonate biodeposition, *Constr. Build. Mater.* 34 (2012) 145–150.
- [21] W. De Muynck, D. Debrouwer, N. De Belie, W. Verstraete, Bacterial carbonate precipitation improves the durability of cementitious materials, *Cem. Concr. Res.* 38 (2008) 1005–1014.
- [22] R. Kumar, B. Bhattacharjee, Porosity, pore size distribution and in situ strength of concrete, *Cem. Concr. Res.* 33 (2003) 155–164.
- [23] P. Tiano, L. Biagiotti, G. Mastromei, Bacterial bio-mediated calcite precipitation for monumental stones conservation: methods of evaluation, *J. Microbiol. Methods* 36 (1999) 139–145.
- [24] V. Achal, A. Mukherjee, P.C. Basu, M.S. Reddy, Lactose mother liquor as an alternative nutrient source for microbial concrete production by *Sporosarcina pasteurii*, *J. Ind. Microbiol. Biotechnol.* 36 (2009) 433–438.
- [25] S. Ghosh, M. Biswas, B. Chattopadhyay, S. Mandal, Microbial activity on the microstructure of bacteria modified mortar, *Cem. Concr. Compos.* 31 (2009) 93–98.
- [26] P. Li, C. Liu, W. Zhou, Improved strength and durability of concrete by bacterial carbonate precipitation, 2015.
- [27] A.A. Ramezani-pour, S.A. Ghahari, M. Esmaeili, Effect of combined carbonation and chloride ion ingress by an accelerated test method on microscopic and mechanical properties of concrete, *Constr. Build. Mater.* 58 (2014) 138–146.
- [28] F.P. Glasser, K. Luke, M.J. Angus, Modification of cement pore fluid compositions by pozzolanic additives, *Cem. Concr. Res.* 18 (1988) 165–178.
- [29] P.D. Tennis, H.M. Jennings, A model for two types of calcium silicate hydrate in the microstructure of Portland cement pastes, *Cem. Concr. Res.* 30 (2000) 855–863.
- [30] F. Lin, C. Meyer, Hydration kinetics modeling of Portland cement considering the effects of curing temperature and applied pressure, *Cem. Concr. Res.* 39 (2009) 255–265.
- [31] T. Bier, J. Kropp, H. Hilsdorf, Formation of silica gel during carbonation of cementitious systems containing slag cements, in: Third International Conference Proceedings Fly Ash, Silica Fume, Slag, and Natural Pozzolans in Concrete, 1989.

- [32] J.H. Adair, E. Suvaci, Morphological control of particles, *Curr. Opin. Colloid Interface Sci.* 5 (2000) 160–167.
- [33] C. Lu, L. Qi, H. Cong, X. Wang, J. Yang, L. Yang, D. Zhang, J. Ma, W. Cao, Synthesis of calcite single crystals with porous surface by templating of polymer latex particles, *Chem. Mater.* 17 (2005) 5218–5224.
- [34] M. Dittrich, S. Sibler, Cell surface groups of two picocyanobacteria strains studied by zeta potential investigations, potentiometric titration, and infrared spectroscopy, *J. Colloid Interface Sci.* 286 (2005) 487–495.
- [35] I.W. Sutherland, Biofilm exopolysaccharides: a strong and sticky framework, *Microbiology* 147 (2001) 3–9.
- [36] V.R. Phoenix, D.G. Adams, K.O. Konhauser, Cyanobacterial viability during hydrothermal biomineralisation, *Chem. Geol.* 169 (2000) 329–338.
- [37] R. Sekar, V.P. Venugopalan, K.K. Satpathy, K.V.K. Nair, V.N.R. Rao, Laboratory studies on adhesion of microalgae to hard substrates, *Hydrobiologia* 512 (2004) 109–116.
- [38] O.S. Pokrovsky, R.E. Martinez, S.V. Golubev, E.I. Kompantseva, L.S. Shirokova, Adsorption of metals and protons on *Gloeocapsa* sp. cyanobacteria: a surface speciation approach, *Appl. Geochem.* 23 (2008) 2574–2588.
- [39] A. Bains, N.K. Dhami, A. Mukherjee, M.S. Reddy, Influence of exopolymeric materials on bacterially induced mineralization of carbonates, *Appl. Biochem. Biotechnol.* 175 (2015) 3531–3541.
- [40] K.L. Gallagher, O. Braissant, T.J. Kading, C. Dupraz, P.T. Visscher, Phosphate-related artifacts in carbonate mineralization experiments, *J. Sediment. Res.* 83 (2013) 37–49.